Complexity and regularity of vector-soliton collisions

Yu Tan and Jianke Yang
Department of Mathematics and Statistics, University of Vermont, Burlington, Vermont 05401
(Received 5 June 2001; revised manuscript received 30 June 2001; published 24 October 2001)

In this paper, we extensively investigate the collision of vector solitons in the coupled nonlinear Schrödinger equations. First, we show that for collisions of orthogonally polarized and equal-amplitude vector solitons, when the cross-phase modulational coefficient β is small, a sequence of reflection windows similar to that in the ϕ^4 model arises. When β increases, a fractal structure unlike ϕ^4's gradually emerges. But when β is greater than one, this fractal structure disappears. Analytically, we explain these collision behaviors by a variational model that qualitatively reproduces the main features of these collisions. This variational model helps to establish that these window sequences and fractal structures are caused entirely or partially by a resonance mechanism between the translational motion and width oscillations of vector solitons. Next, we investigate collision dependence on initial polarizations of vector solitons. We discovered a sequence of reflection windows that is *phase induced* rather than resonance induced. Analytically, we have derived a simple formula for the locations of these phase-induced windows, and this formula agrees well with the numerical data. Last, we discuss collision dependence on relative amplitudes of initial vector solitons. We show that when vector solitons have different amplitudes, the collision structure simplifies. Feasibility of experimental observation of these results is also discussed at the end of the paper.

DOI: 10.1103/PhysRevE.64.056616 PACS number(s): 42.65.Tg, 05.45.Yv, 42.81.Dp

I. INTRODUCTION

Collision of solitary waves is an important problem for both physical and mathematical reasons. Physically, solitary-wave collisions are common phenomena in science and engineering. For instance, a popular technology in fiber communication systems is wavelength-division multiplexing (WDM). In a WDM system, optical pulses in different frequency channels collide with each other all the time [1–3]. In waveguides such as crystals, photorefractives, and air, beam collision is being utilized to achieve instant beam steering and control [4–10]. Water-wave collisions in the ocean and on the beach are even more familiar [11]. Mathematically, solitary-wave collision is a major branch of nonlinear waves. In integrable systems, solitary waves collide elastically. But if the system is nonintegrable, this collision may be highly nontrivial. Much work has been done on solitary-wave collisions in a large array of physical systems. Various collision scenarios such as transmission, reflection, annihilation, trapping, creation of solitary waves and even mutual spiraling have been reported [12–20]. In particular, for kink-antikink collisions in the ϕ^4 and related models, an interesting sequence of resonant reflection windows has been discovered [21–25]. Near the edge of each resonance window, other sequences of resonant windows with more ''bouncing'' have also been revealed [22,23,26]. This phenomenon is the so-called fractal structure in ϕ^4-related systems. In two recent articles, we found a somewhat different fractal structure in vector-soliton collisions in the nonintegrable coupled nonlinear Schrödinger (NLS) equations [27,28]. When we zoom in to various collision-velocity windows, we obtain a copy, a horizontal reflection, or a vertical reflection of the original graph with all the major geometric features preserved. Unlike the ϕ^4 fractal, zooming operations for the vector-soliton fractal are performed not at edges of a resonant window. More importantly, the basic structure of this coupled NLS fractal is a sequence of multipass and multibounce windows, while the basic structure of the ϕ^4 fractal is a collection of two-pass windows. Very recently, breather interactions in a weakly discrete sine-Gordon equation have been studied, and a fractal structure has been identified there as well [20].

The fractal dependence is probably the most vivid manifestation of both complexity and regularity in solitary-wave collisions. Such dependence in the coupled NLS equations is particularly significant since those equations directly govern pulse propagation in birefringent fibers and WDM systems [1,2,29]. Those equations are also closely related to beam propagation in crystals and photorefractive waveguides [10]. In [27,28], this fractal structure was shown only for one cross-phase modulational (XPM) coefficient $\beta=2/3$ that corresponds to linear fiber birefringence. In addition, only collisions of vector solitons with equal amplitudes and orthogonal polarizations were studied. In engineering applications, elliptical fiber birefringence is not uncommon [30]. Furthermore, initial solitons are not always in orthogonal polarizations or with equal amplitudes. Thus, how this fractal structure changes when the XPM coefficient, initial polarizations, and relative amplitudes vary is obviously a pressing question. In addition, in [27,28], the mechanism for this fractal dependence was argued as a resonance between the translational motion and internal oscillations of vector solitons on numerical and heuristic grounds. A more quantitative analytical theory to explain this fractal structure is clearly called upon. All these important questions will be addressed in the present paper.

The results of this paper may be summarized as follows. We first investigate the collision dependence of orthogonally polarized and equal-amplitude vector solitons on the XPM coefficient $\beta(>0)$. We find that when β is very small, vector solitons pass through each other at collision velocities V_0 above a critical value V_c, and trap each other at collision

velocities $V_0 < V_c$. When β increases, a sequence of reflection windows similar to that in the ϕ^4 model gradually emerges just below the critical velocity V_c. In all these windows, the two solitons pass each other only twice, but numbers of width oscillations of vector solitons (or equivalently, collision time) between the two passes differ. When β increases further, a fractal structure unlike ϕ^4's emerges [27]. As β approaches one, this fractal structure simplifies. When $\beta=1$ (the Manakov model), the collision is elastic and complexity disappears. When $\beta>1$, the collision is not elastic, but the collision structure remains simple. Theoretically, we explain the above intricate collision structure and dynamics by a simple variational model. With this model, we succeeded in qualitatively reproducing the key features of vector-soliton collisions in the original partial differential equations (PDE's). This success helps to establish that the mechanism for window sequences and fractal structures in vector-soliton collisions may be attributed to a resonance between the translational motion and width oscillations (breathing) of colliding solitons. Next, we investigate collision dependence on initial polarizations of vector solitons. In this case, we discovered a sequence of reflection windows that is quite different from that in the collision of orthogonally polarized vector solitons. Collisions in these windows are all simple and also similar to each other. We will show that this window sequence is not induced by a resonance mechanism. Rather, it is phase induced, i.e., it is caused by the collision's dependence on vector solitons' relative phases. Analytically we derived a simple formula for the window locations in this sequence, and it agrees well with the numerical data. Last, we study collision dependence on relative amplitudes of initial solitons. We find that when vector solitons have different amplitudes, the collision structure simplifies.

Complexity of vector-soliton collisions is remarkable enough. Equally remarkable is the clear pattern and regularity in these collisions. In addition to the fractal structure that exhibits clear patterns amidst complicated collisions, we also find that window locations in a sequence are given by simple formulas as well. Specifically, in the window sequence for collisions of orthogonally polarized vector solitons at small β values, quantity $(V_c^2-V_n^2)^{-1/2}$, where V_c is the critical velocity and V_n is the center of the nth window, is a linear function of the window index n. In the window sequence for collisions of nonorthogonally polarized vector solitons, V_n^{-1} is a linear function of n. We also find that in the window sequence for orthogonally polarized vector solitons, the collision time T_n depends linearly on n. These surprisingly simple formulas testify to the high regularity of vector-soliton collisions. It is noted that the linear dependence of quantity $(V_c^2-V_n^2)^{-1/2}$ and collision time T_n on window index n occurs in the ϕ^4-related models as well [21–25]. Hence, this dependence appears to be universal in resonance-induced window sequences.

The structure of this paper is organized as follows. In Sec. II, we study the collision dependence of orthogonally polarized and equal-amplitude vector solitons on XPM coefficient β (>0). In Sec. III, we present a variational model that qualitatively explains the collision structure and dynamics of Sec. II. In Secs. IV and V, we examine the collision dependence on polarizations and relative amplitudes, respectively. In Sec. VI, we summarize our main results, and argue that the experimental observation of our results is feasible.

II. COLLISIONS OF ORTHOGONALLY POLARIZED AND EQUAL-AMPLITUDE VECTOR SOLITONS

The coupled NLS equations under study are

$$iA_t + A_{xx} + (|A|^2 + \beta|B|^2)A = 0, \tag{2.1}$$

$$iB_t + B_{xx} + (|B|^2 + \beta|A|^2)B = 0, \tag{2.2}$$

where A and B are complex amplitudes of wave envelopes in two orthogonal polarizations or two WDM channels [3,29]. The parameter β is the XPM coefficient that is always positive in optics applications. The system (2.1) and (2.2) is phase, position, and Galilean invariant. Solitary waves in this system are of the form

$$A(x,t) = r_1(x - vt - x_0)e^{(1/2)ivx + i[\omega_1^2 - (v^2/4)]t + i\gamma_1}, \tag{2.3}$$

$$B(x,t) = r_2(x - vt - x_0)e^{(1/2)ivx + i[\omega_2^2 - (v^2/4)]t + i\gamma_2}, \tag{2.4}$$

where ω_1^2 and ω_2^2 are frequencies of the A and B components, and initial position x_0, velocity v, phases γ_1, γ_2 are arbitrary parameters. In the optics literature, these solitary waves are called vector solitons even though their collisions generally are not elastic at all. The real-valued amplitude functions $r_1(x)$ and $r_2(x)$ are related to frequencies ω_1^2 and ω_2^2 through the following ordinary differential equations (ODE's):

$$r_{1xx} - \omega_1^2 r_1 + (r_1^2 + \beta r_2^2)r_1 = 0, \tag{2.5}$$

$$r_{2xx} - \omega_2^2 r_2 + (r_2^2 + \beta r_1^2)r_2 = 0. \tag{2.6}$$

This ODE system supports a wide array of solitary-wave solutions. The single-humped vector solitons are linearly stable, and all the others are believed to be linearly unstable [31–34]. In this paper, we only consider collisions of single-humped vector solitons. Such solitons are of two types. One type is degenerate where either the A or B component vanishes. In this case, the other component is simply a NLS soliton that has a sech profile. The other type is true vector solitons where both A and B components are nonzero. Such solitons exist only when the frequency ratio ω_2/ω_1 falls between two values $(\sqrt{1+8\beta}-1)/2$ and $2/(\sqrt{1+8\beta}-1)$ [15,32]. In general, these solitons defy explicit analytical expressions and have to be determined numerically.

In this section, we focus on the collision of orthogonally polarized and equal-amplitude vector solitons. These collisions arise often in WDM systems and photorefractive materials [3,5]. The initial conditions for such collisions may be written as

$$A(x,0) = \sqrt{2}\ \operatorname{sech}\left(x + \frac{1}{2}\Delta_0\right)e^{(1/4)iV_0 x}, \tag{2.7}$$

$$B(x,0)=\sqrt{2}\ \ \mathrm{sech}\left(x-\frac{1}{2}\Delta_0\right)e^{-(1/4)iV_0x}, \qquad (2.8)$$

where $V_0(>0)$ is the relative velocity of the two initial solitons, and $\Delta_0(\gg 1)$ is the initial separation. In other words, initially, the two-vector solitons are both degenerate, but the left soliton (2.7) is polarized entirely in the A component, and the right soliton (2.8) is polarized in the B component. For convenience, we will call the left soliton as A pulse, and the right soliton as B pulse. These pulses initially move toward each other at relative velocity V_0. This velocity will be called collision velocity throughout this article. Due to phase invariances of Eqs. (2.1) and (2.2), any initial phases in the two solitons (2.7) and (2.8) may be removed. The amplitudes of these solitons are equal and have been normalized to $\sqrt{2}$ without loss of generality. The collision results of these solitons do not depend on the specific value of Δ_0 as long as it is large enough. It is noted that with the present initial condition, solutions $A(x,t)$ and $B(x,t)$ are related by a simple symmetry: $B(x,t)=A(-x,t)$. Because of this, only contours of the A component are shown in this section, as the contours of the B component may be obtained by a simple mirror reflection of A contours about position $x=0$. When $\beta=0$ or 1 (integrable cases), the two NLS solitons (2.7) and (2.8) will simply pass through each other without change in amplitude, velocity, or polarization [35–37]. In the Manakov case ($\beta=1$), polarization rotations do not occur here because initial solitons are orthogonally polarized [36,37]. When $\beta\neq 0$ and 1 (nonintegrable case), amplitudes, velocities, and polarizations of initial solitons will all change after collision. This nonintegrable collision will be the focus of study in this section.

At each XPM coefficient β, we have simulated Eqs. (2.1) and (2.2) extensively with initial conditions (2.7) and (2.8), using collision velocity V_0 as a control parameter. We take $\Delta_0=20$ which proves to be large enough for the results we report in this section. The numerical scheme we use is a third-order split-step method. The x interval was taken as $[-80,80]$, and 1024 grid points were used. The time step was taken as 0.01. To minimize radiation that can feed back into the system through periodic boundary conditions, a damping condition has been applied in the boundary intervals $[-80,-60]$ and $[60,80]$. To assess numerical errors, we have selectively run our simulations with wider x intervals, larger grid points, and smaller time steps. The results show that our choice of scheme parameters are adequate. As an independent check, we have also written a code that uses the pseudospectral method along the x direction and fourth-order Runge-Kutta method to advance in time. Our extensive comparisons of these two numerical schemes show no disagreement. All our simulations used double precision (about 16 significant digits).

Our numerical simulations reveal three collision scenarios: transmission, reflection, and trapping. In a transmission scenario, most energy in the pulses (2.7) and (2.8) passes through. In a reflection scenario, most energy in the two pulses is reflected back. In a trapping scenario, the two pulses trap each other and form a bound state. When the collision is transmissional or reflectional, we have found that only two-vector solitons emerge out of collision, unless the XPM coefficient β is relatively large ($\gtrsim 2$). Polarizations of these two exit vector solitons generally are different from 0 and $\pi/2$ of the initial solitons'. This phenomenon is the so-called shadow formation in the literature. In each collision, radiation of various amount is also observed. We note that in some rare cases, the transmitted energy and reflected energy of pulses (2.7) and (2.8) are almost equal. When this happens, the two exit solitons both have approximately 45° polarization angles. In such cases, the distinction between transmissional and reflectional collisions is blurred (see Fig. 6). We define the exit velocity V of a transmissional or reflectional collision as the relative separation velocity of the two exit solitons. For transmissional collision, V is positive. For reflectional collision, V is negative. In a trapping collision, we simply assign V as zero. To determine exit velocities numerically, we simulate each collision for a long time. Meanwhile, we track the positions of $|A|$ and $|B|$'s maximum values. After a long-time simulation, if these two positions still remain very close to each other, we decide that the solitons (2.7) and (2.8) have trapped each other and set exit velocity as zero. Otherwise, we use the statistical least-squares method to fit the velocities of $|A|$ and $|B|$'s maximum-value positions. The difference between these two velocities is recorded as the exit velocity. Due to the symmetry of the initial condition (2.7) and (2.8), these two velocities must be opposite to each other. This relation serves as an additional check of our numerical accuracy.

We have carried out collision simulations of solitons (2.7) and (2.8) for a large number of β values ranging from 0 to 2. Below, we will present collision results at selected β values that highlight the main features of collision structure and dynamics as β continuously increases from zero. Results at other β values will not be displayed but briefly described. To restrict the scope of this paper, we will only report exit-velocity results for each case with the only exception at the physically significant value $\beta=2$, where component amplitudes of exit pulses are also presented [see Fig. 7(b)]. At another physically significant XPM coefficient $\beta=2/3$, component amplitudes of exit pulses may be found in [28].

A. $\beta=0.05$

When $\beta=0$, the system (2.1) and (2.2) is decoupled. Solitons (2.7) and (2.8) do not interact with each other, and there is no collision. So, the exit-velocity V is always exactly equal to the collision-velocity V_0. When β increases from 0, the first nontrivial phenomenon is that, at small collision velocities, solitons (2.7) and (2.8) trap each other and form a bound state. At $\beta=0.05$, the exit-velocity versus collision-velocity graph is shown in Fig. 1(a). As we can see, when V_0 is smaller than a critical velocity $V_c=0.1715$, trapping collision always occurs. Here, the critical-velocity V_c is defined as the smallest collision velocity above which all collisions are transmissional. This definition will be used throughout this paper. To demonstrate, we take $V_0=0.1$, and show the $|A|$ contour of the collision in Fig. 1(b). We remind the reader that the $|B|$ contour is just a horizontal reflection of

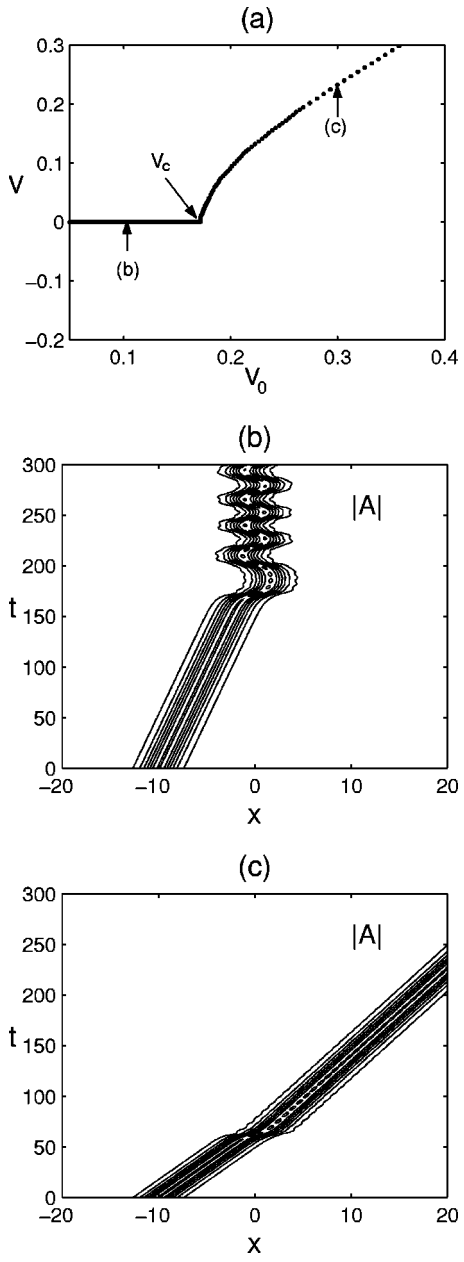

FIG. 1. Collision results for $\beta=0.05$: (a) exit-velocity graph; (b, c) $|A|$ contours at collision velocities marked by respective letters in (a). Contour levels are both 0.2:0.2:1.4.

the $|A|$ contour about $x=0$ axis. We see in this figure that after the first pass, the two solitons are dragged toward each other. Then they trap each other and engage in internal oscillations [38–41]. In this collision, translational energy of initial solitons has been transferred into internal-oscillation energy. Small amount of radiation is emitted as well. We note in passing that the state of internal oscillations in this graph may last for a very long time. But, eventually these oscillations will decay algebraicly due to radiation damping, and the solution asymptotically approaches a stationary vector-soliton state [40,42]. When $V_0>V_c$, the collision is transmissional. An example is shown in Fig. 1(c) with $V_0=0.3$. Note that the solitons slow down a bit after collision. In addition, their amplitudes and widths oscillate mildly. These oscillations decay over time. The energy radiation caused by the collision is very small here (less than 1%). At higher β values (to be discussed below), energy radiation may increase slightly. But the radiation amount is still less than 10% in most cases.

B. $\beta=0.2$

As β increases from 0.05, a very interesting phenomenon happens. That is, a sequence of reflection windows gradually appears just below the critical-velocity V_c. At $\beta=0.2$, this phenomenon is displayed in Fig. 2(a). Note that these reflection windows are intertwined with trapping intervals. In addition, they are spaced closer and become narrower as collision-velocity V_0 approaches the critical-velocity V_c, which is equal to 0.935 63 in Fig. 2(a). A note-worthy fact is that, as β increases from 0.05 to 0.2, reflection windows closer to the critical velocity V_c appear first. Windows further away (to the left) from the critical velocity appear later. This explains why in Fig. 2(a), the first window on the far left is so low since it was just born. No other reflection windows were found below $V_0=0.9$ in Fig. 2(a).

An important characteristic of this sequence of reflection windows is that quantity $(V_c^2-V_n^2)^{-1/2}$, where V_c is the critical velocity and V_n is the midpoint of the nth window, is almost a perfect linear function of the window index n, i.e.,

$$(V_c^2-V_n^2)^{-1/2}=\mu n+\theta, \tag{2.9}$$

where μ and θ are constants. To demonstrate this, we first assign $n=2,3,\ldots,$ for the reflection windows in Fig. 2(a) starting from the left. The reason we did not assign $n=1$ to the first window in Fig. 2(a) is that, an even lower window in this sequence does exist not at $\beta=0.2$, but at higher β values. That window should be the first in this sequence of reflection windows and should be given index $n=1$. After assignment of window indices, we numerically determine each window's midpoint V_n, which is almost the same as the bottom point of that window. Then we plot the quantity $(V_c^2-V_n^2)^{-1/2}$ versus window index n in Fig. 2(b) (circles). We see that these points fall onto a straight line almost perfectly. A least-square line fit gives the slope μ and y-intercept θ as

$$\mu=2.0588, \quad \theta=0.0375. \tag{2.10}$$

Collision dynamics in this sequence of reflection windows is very interesting. It turns out that in all these reflection windows, the two solitons pass each other only twice. But the time between these two passes varies from one window to another. In addition, solitons between passes show a significant amount of width and amplitude oscillations. To illustrate, we pick the bottom points of windows with indices $n=3$ and 6 in Fig. 2(a), and display their collision contours in Figs. 2(c) and 2(d), respectively. We see that in both cases, solitons pass each other twice: the first pass occurs when they come together, and the second pass occurs when they escape from each other. But numbers of width oscillations between the two passes are different. These features are

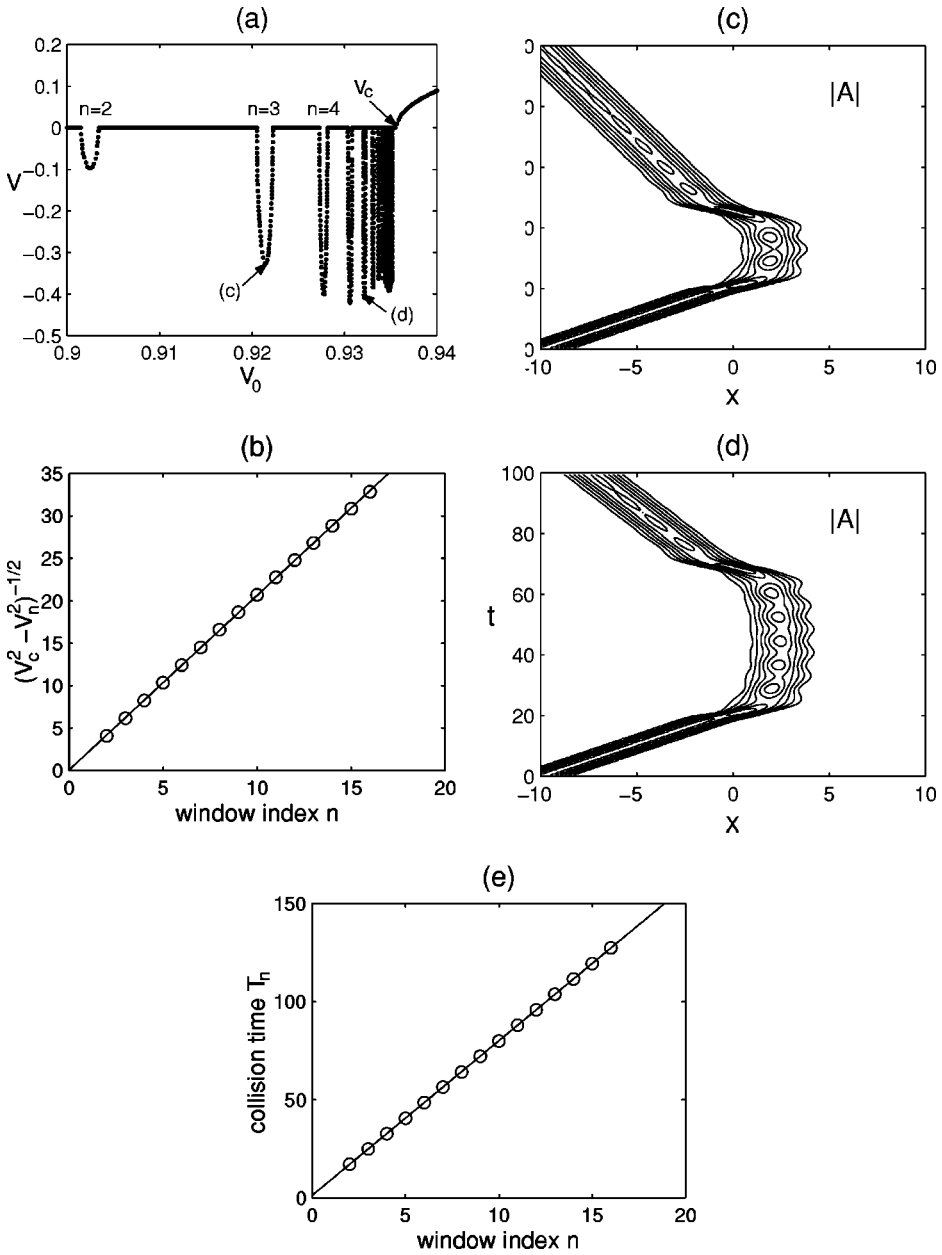

FIG. 2. Collision results for $\beta = 0.2$. (a) Exit-velocity graph. (b) $(V_c^2 - V_n^2)^{-1/2}$ graph (circles). The solid line is the least-squares fit given by Eqs. (2.9) and (2.10). (c, d) $|A|$ contours with V_0 at the bottoms of the second and fifth windows with indices $n=3$ and 6 in (a). Contour levels are both 0.6:0.15:1.35. (e) Collision time graph (circles). The solid line is the least-squares fit given by Eqs. (2.11) and (2.12).

common to all those reflection windows. Below, we will call these reflection windows as two-pass windows.

Why do these reflection windows appear amidst trapping intervals? The answer is suggested by Figs. 2(c) and 2(d). We see that during collisions, each soliton still holds up (no splitting), but its amplitude and width oscillate considerably (breathing). After collision, these oscillations become much weaker. This suggests an energy exchange mechanism between solitons' translational motion and width oscillations. This energy exchange would be the strongest if time between the two passes is multiples of the width-oscillation period (plus a constant offset parameter to account for intricacies near the passes). In other words, we expect that

$$\omega T_n = 2n\pi + \delta, \tag{2.11}$$

where T_n is the time between two passes when the collision velocity V_0 is at the bottom of the nth window, ω is the width oscillation frequency, and δ is an offset parameter. This turns out to be the case indeed. When collision time T_n, which is measured numerically as the time between the two intersections of $|A|$ and $|B|$'s maximum-value positions, is plotted versus window index n in Fig. 2(e) (circles), these points fall onto a straight line very nicely. A least-square line fit of this data gives frequency ω and offset parameter δ as

$$\omega = 0.7976, \quad \delta = 0.9764. \tag{2.12}$$

An analytical study of the above sequence of reflection windows will be carried out in Sec. III.

At this moment, we would like to draw the reader's attention to the remarkable similarity between collisions of Fig. 2 and those of kink-antikink collisions in ϕ^4-related models [21–26]. First of all, ϕ^4 models also have a sequence of reflection windows just like Fig. 2(a). Second, collision dy-

namics in ϕ^4 models is analogous to that in Figs. 2(c) and 2(d). Third, locations of reflection windows in ϕ^4 models have the same functional form as Eq. (2.9). Fourth, collision time in ϕ^4 models is given by the same formula (2.11). Fifth, the mechanism for those reflection windows in ϕ^4 models is a resonance between translational motion and internal (shape) modes of kinks and antikinks, similar to the one for our model. Even though kinks and antikinks are topological solitons that have infinite mass, while solitons (2.7) and (2.8) are localized entities, similarities of collision dynamics between them are surprising. A minor difference between resonance mechanisms of these two models is worth mentioning. In the ϕ^4 models, the resonance is with internal modes of kinks and antikinks. These modes are discrete eigenfunctions of ϕ^4 models linearized around kinks and antikinks. In the present paper, width oscillations of solitons as seen in Figs. 2(c) and 2(d) are due to radiation modes [43]. Thus, the resonance here is with radiation modes of solitons. Since radiation modes exist in every conservative wave system, while internal modes are relatively rare, we believe that resonance with radiation modes is more common in physical wave systems.

A visually distinctive difference between the collision structure of Fig. 2(a) and that of ϕ^4 models is that, in ϕ^4 models, at the edge of each reflection window, another sequence of windows with one more ''bouncing'' can be found [21,26]. In Fig. 2(a), we do not see such edge sequences. This is not because we missed such edge windows in our numerics. Rather, the reason is energy radiation, which wipes out such edge windows. However, remnants of such edge windows still persist in the present collisions. For instance, we take the window with index n=3 in Fig. 2(a) and select two collision velocities 0.920 22 and 0.920 49 just below its left edge. Collision contours at these two velocities are shown in Figs. 3(a) and 3(b). In both contours, we see that the initial collision dynamics is almost the same as that in Fig. 2(c), obviously because these two collision velocities are so close to the left edge of the $n=3$ window in Fig. 2(a). But then instead of escaping, the two solitons in Figs. 3(a) and 3(b) engage in different numbers of width oscillations, followed by a third pass. If solitons escaped after this pass, we would have observed edge windows as in ϕ^4 models. But solitons after the third pass seem to have lost too much energy to escape. So they subsequently trap each other and form a bound state. This is the only difference on edge collisions between ϕ^4 and our models. At $\beta=0.2$, those edge windows did not come out. However, when β gets larger (say 0.6 or 2/3), edge windows of one more pass do finally appear. It is helpful to note here that in the variational model of Sec. III where energy is never radiated, sequences of edge windows indeed exist at $\beta=0.2$ (see Fig. 9).

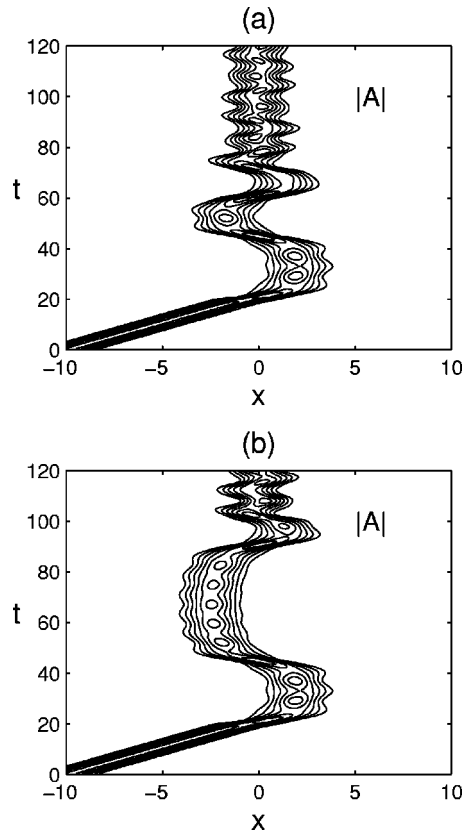

FIG. 3. Collision contours ($|A|$) at two velocities just below the second reflection window (with index $n=3$) in Fig. 2(a): (a) $V_0=0.920\,22$; (b) $V_0=0.920\,49$. Both contours are at levels 0.6:0.15:1.35.

C. $\beta=0.6$

As β increases from 0.2, the two-pass windows of Fig. 2(a) move closer to the critical-velocity V_c, and the lowest two-pass window with index $n=1$ finally emerges at a β value somewhere between 0.3 and 0.4. After it is born, the sequence of two-pass windows is then complete. If β increases further, a pass-bounce-pass window appears on the left of the two-pass window sequence. The collision dynamics of this pass-bounce-pass window is as shown in Fig. 4(c) described below. In addition, this pass-bounce-pass window starts to develop its own sequence of windows inside the two-pass window sequence. Meanwhile, other windows of even more complex collisions continue to emerge. Here, by a window sequence, we mean a sequence of windows whose collision dynamics are the same, except that numbers of width and position oscillations at a certain stage of the collision are different (see Figs. 2 and 4). These developments subsequently lead to the fractal structure reported in [27]. That is, when we zoom into the neighborhood of higher-indexed two-pass windows, we get a copy of the entire structure (qualitatively). This development is illustrated in Fig. 4 at $\beta=0.6$. The whole exit velocity graph is displayed in Fig. 4(a). The wide reflection window whose bottom is marked by letter ''(c)'' is the simplest pass-bounce-pass window. The other wide reflection window whose bottom is marked by letter ''(d)'' is the simplest two-pass window with index $n=1$. Collision contours at the bottoms of these two windows are shown in Figs. 4(c) and 4(d), respectively. Now, if we zoom into the neighborhood of the second two-pass window, specifically, we zoom into the interval [1.265 50, 1.267 15], which is highlighted by two vertical dashed lines in Fig. 4(a), we get Fig. 4(b), which is roughly a copy of Fig.

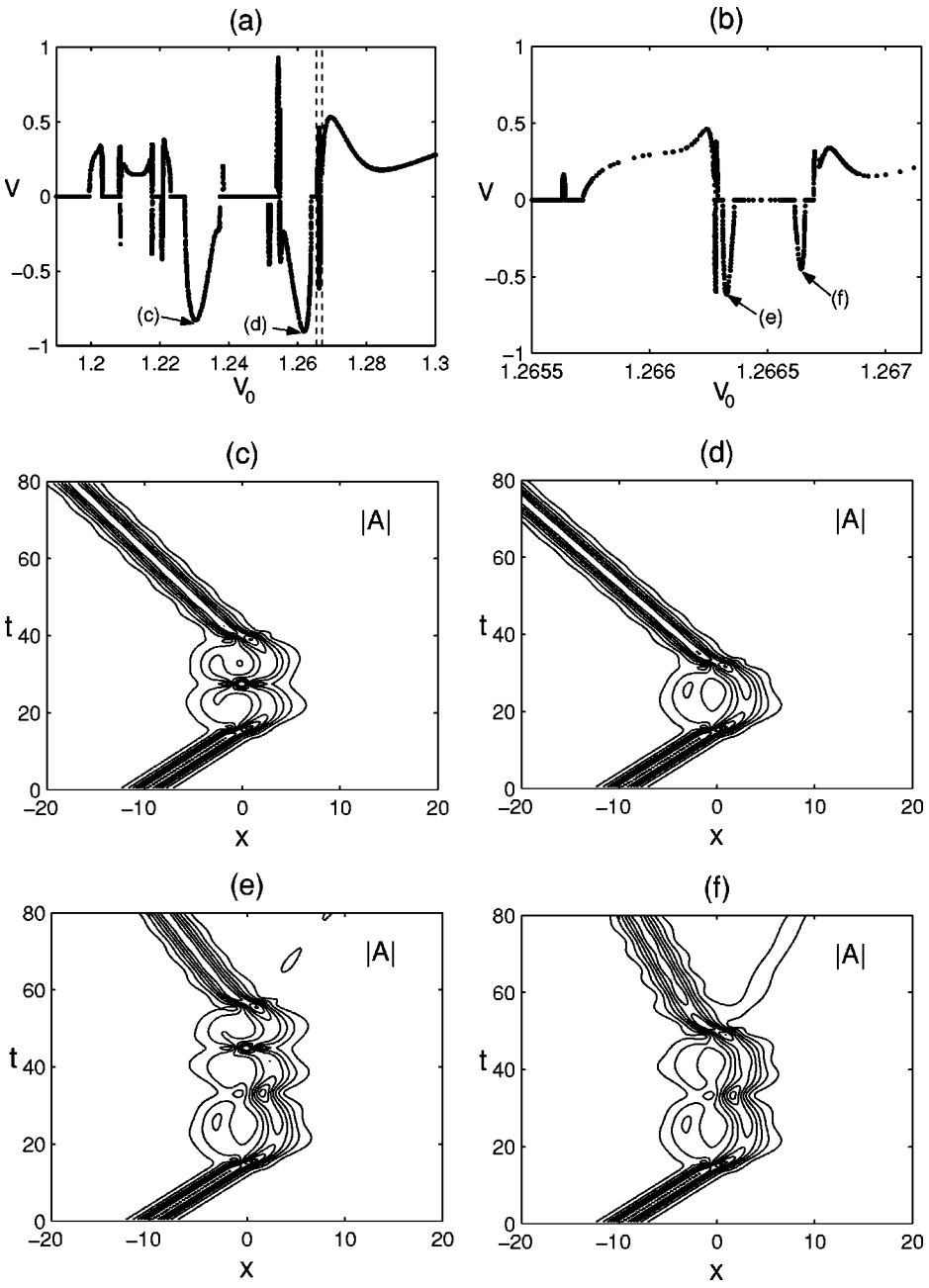

FIG. 4. Collision results for $\beta = 0.6$. (a) Exit-velocity graph; (b) enlargement of the interval marked by two vertical dashed lines in (a); (c,d,e,f): $|A|$ contours with collision velocities V_0 at the bottoms of the reflection windows marked by respective letters in (a) and (b). All contours are 0.2:0.2:1.4.

4(a). Thus, Fig. 4(a) has a fractal structure. Note that this zoomed-in window preserves the main features of Fig. 4(a). In particular, we see counterparts of pass-bounce-pass window in Fig. 4(a) and two-pass window in Fig. 4(b) [marked by (e) and (f), respectively]. Collision dynamics at the bottoms of these two reflection windows in Fig. 4(b) are displayed in Figs. 4(e) and 4(f). Comparing Figs. 4(c) and 4(d) with 4(e) and 4(f), we see clearly that the reflection window marked by ''(f)'' in Fig. 4(b) is the next two-pass window with index $n=2$, and the reflection window marked by ''(e)'' in that figure is the next pass-bounce-pass window. Notice that in Figs. 4(e) and 4(f), after the first pass, solitons oscillate once about their positions. The rest of the collisions are qualitatively the same as those in Figs. 4(c) and 4(d). This pattern is true everywhere in Fig. 4(a) and its zoomed-in window Fig. 4(b). In other words, at the same relative positions of Figs. 4(a) and 4(b), the collision in Fig. 4(b) is just one more oscillation after the first pass. The rest of the collision is the same as that in Fig. 4(a). A similar finding has been reported in [27,28] at $\beta=2/3$. There are some minor but significant differences between Figs. 4(a) and 4(b). First, the left end of Fig. 4(a) is broken into a few pieces, while at the same position in Fig. 4(b), the structure is a rather smooth curve. As β increases from 0.6, these broken pieces in Fig. 4(a) do merge into a smooth curve (see [28]). Another difference is that some windows in Fig. 4(a) get lost in the zoomed-in window in Fig. 4(b). For instance, the high transmission window in the center region of Fig. 4(a) disappears in Fig. 4(b).

The collision structure in Fig. 4(a) is actually much richer than those reported above. First, at the lower edge of the simplest two-pass window [marked by ''(d)'' in that figure]

and at the upper edge of the simplest pass-bounce-pass window [marked by ''(c)'' there], windows of one more pass (transmission windows) finally emerge. These edge windows are hallmarks of ϕ^4 fractals [21,26]. At $\beta=0.2$, when we see a beautiful two-pass window sequence similar to ϕ^4's in Fig. 2(a), such edge windows did not appear due to energy radiation. But now they have. Second, some of the newly emerged windows cluster together and form other structures. When we zoom into such structures, we get pictures that are related to the whole picture. An example is the cluster in the interval [1.215, 1.224] on the left of the pass-bounce-pass window marked by ''(c)'' in Fig. 4(a). When we zoom into this cluster, the graph we get is qualitatively a horizontal reflection of the original graph [it looks very much like a reflection of Fig. 4(b)]. Collision dynamics in this zoomed-in window is also closely related to that in the original graph. This phenomenon has been reported in [28], thus details will be omitted here. Another example is the cluster in the interval [1.198, 1.213] which is on the far left of Fig. 4(a). Zooming into different locations of this cluster produces a copy or horizontal reflection of this cluster itself. In addition, these zoomed-in graphs bear similarities to the whole structure of Fig. 4(a).

To conclude this section, we would like to emphasize the difference between ϕ^4 fractals and our present coupled NLS fractal. In ϕ^4 fractals, the basic structure is a sequence of two-pass windows just like Fig. 2(a), all of which have two-pass collisions of varying collision times [21–25]. At the edge of a two-pass window, a sequence of three-pass windows may be found [21,26]. These edge-window sequences make the ϕ^4 collision structure a fractal. In the coupled NLS fractal, the basic structure is *not* the sequence of two-pass windows. Rather, it is a collection of windows whose collisions have various numbers of passing and bouncing. In other words, complex collisions directly enter the basic structure of the coupled NLS fractal. Our zooming operation is not at the edge of a two-pass window either. In addition, in zoomed-in windows, collision dynamics is not one more pass. Rather, it is one more position oscillation (see Fig. 4). Traces of ϕ^4-type fractals may still be found here through the existence of edge windows just mentioned above (see also Figs. 2 and 3). But that perspective does not capture the main collision structures and dynamics of Fig. 4(a) (see also [27,28]). Thus, that perspective will not be adopted in the rest of this section.

D. $\beta=0.95$

As β continues to increase from 0.6, more reflection and transmission windows emerge. Meanwhile, the broken pieces at the left side of Fig. 4(a) merge together. These developments lead to the fractal structure reported in [27,28] where $\beta=2/3$. When β increases further from 2/3, the fractal structure persists, but the details of this fractal are even more complex. However, when β gets very close to 1 (the Manakov model), the collision structure simplifies. At $\beta=0.95$, the exit-velocity graph is shown in Fig. 5(a). As we can see, all those fractal structures and complicated reflection and transmission windows in Fig. 4(a) have now disappeared.

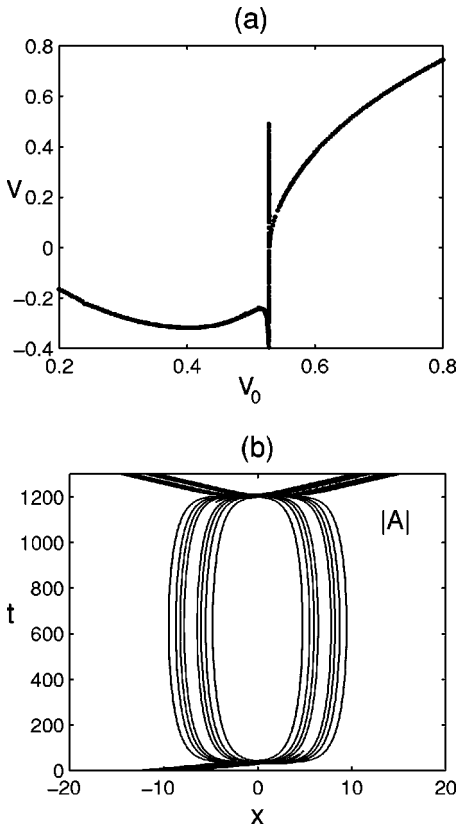

FIG. 5. Collision results for $\beta=0.95$. (a) exit-velocity graph; (b) $|A|$ contour at $V_0=0.528\,45$, which is inside the spike of (a). The contour levels are 0.2:0.2:1.4.

Here, at low-collision velocities, the collision is reflectional, while at high-collision velocities, the collision is transmissional. But the transition from reflectional collisions to transmissional collisions is still nontrivial. In fact, as the reflectional (left) branch and transmissional (right) branch of the exit-velocity curve come toward a critical transition velocity (which is about 0.5283), each branch starts to oscillate more and more rapidly (this oscillation phenomenon has been observed before in [18]). The right branch oscillates between a high-exit velocity of about 0.48 and a low-exit velocity of about 0. The left branch oscillates between a low-exit velocity of about -0.48 and a high-exit velocity of about 0. All these oscillations are very close together so that in Fig. 5(a), those curves appear just as a spike. Collisions inside this spike are very interesting. We found that colliding solitons may form a quasistationary two-vector-soliton bound state for a long time before they eventually separate. To demonstrate, we pick a velocity $V_0=0.528\,45$ inside this spike and display the $|A|$ contour in Fig. 5(b). Here, after solitons come together and pass each other the first time, they form a quasistationary bound state for about 1000 time units. In this bound state, each vector soliton's polarization is very close to 45°. The spacing between the two vector solitons is about 14 units. Phase differences between them are about -1 in the A component, and 1 in the B component. Eventually, the two-vector solitons come together again, pass through each other, and escape. In different cycles of oscillations inside the spike, we have observed different pass/bounce combina-

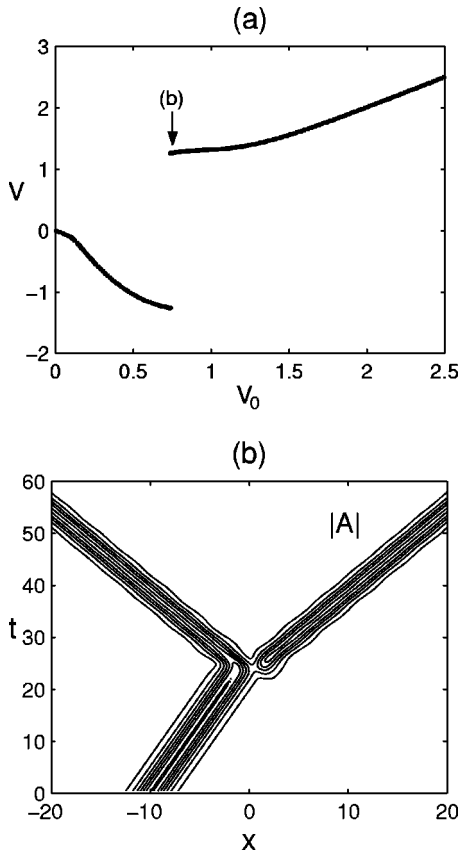

FIG. 6. Collision results for $\beta=1.2$. (a) Exit-velocity graph; (b) $|A|$ contour with V_0 on the right-hand side of the jump in (a). The contour levels are 0.2:0.2:1.4.

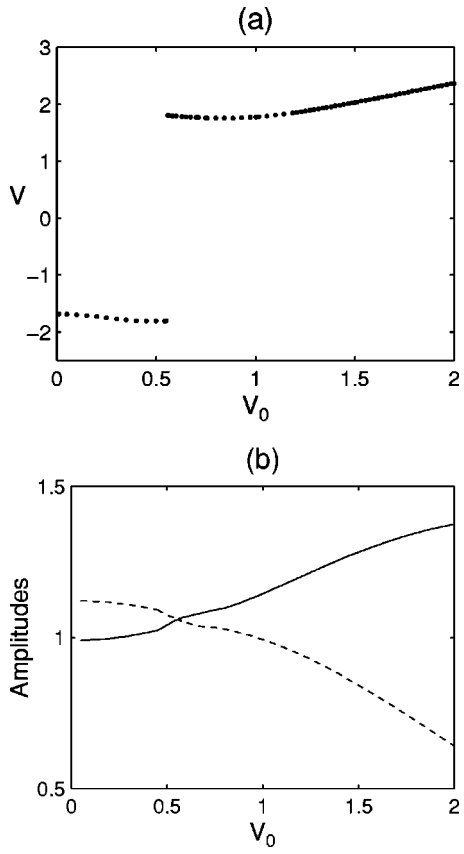

FIG. 7. Collision results for $\beta=2$. (a) Exit-velocity graph; (b) component amplitudes of the right-moving exit vector soliton: solid, *A* component; dashed, *B* component.

tions such as pass-bounce-pass collisions. In each cycle, we found collisions in which a quasistationary two-soliton bound state is present.

E. $\beta=1.2$

When β is equal to 1, the system (2.1) and (2.2) becomes the Manakov model, and the exit velocity becomes identical to the collision velocity everywhere. In other words, the exit velocity graph is a straight line of slope one. When β continues to increase above one, the collision structure remains simple. For instance, at $\beta=1.2$, the exit-velocity graph is shown in Fig. 6(a). Above a critical velocity that is about 0.7403, collisions are all transmissional. Below it, collisions are all reflectional. The transition from reflection to transmission in this figure is a jump. However, this jump is only an artifact of our definitions of reflectional and transmissional collisions. On the right-hand side of the jump, more energy passes through, but the energy that is reflected back is also significant and is comparable to the transmitted energy. This is illustrated in Fig. 6(b), where the $|A|$ contour is displayed at collision velocity $V_0=0.7407$, which is slightly above the jump. Here, the *A*-component amplitude of the left exit-vector soliton is 1.074, and that of the right exit-vector soliton is 1.075. According to our definition, this collision is transmissional, thus, V is positive. When V_0 decreases, the transmitted energy decreases, and the reflected energy increases. At $V_0\approx0.7403$, the transmitted energy is about the same as the reflected energy. As V_0 decreases below 0.7403, more energy is reflected back, thus, collision becomes reflectional, and V becomes negative according to our definition. In short, across this jump in Fig. 6(a), collision does not undergo dramatic qualitative changes. The transition is a smooth one.

F. $\beta=2$

As β increases beyond 1.2, the collision structure always remains simple. For example,, when $\beta=2$, the exit-velocity graph is shown in Fig. 7(a). This figure is as simple as Fig. 6(a). The reason for the jump in Fig. 7 is the same as that in Fig. 6(a): just below the jump, slightly more energy is reflected back; just above the jump, slightly more energy is transmitted through. Since $\beta=2$ is a physically significant value that arises in WDM systems, we have also presented amplitudes of exit-vector solitons in Fig. 7(b). Plotted in this figure are component amplitudes of the right-moving exit-vector soliton. The amplitudes of the left-moving exit-vector soliton may be readily obtained by the symmetry relation $A(x,t)=B(-x,t)$. Polarizations of exit vector solitons can also be inferred from this figure as the arctangent of the amplitude ratios. Figure 7(b) makes the exit velocity jump in Fig. 7(a) easy to understand: across the jump, the relative sizes of component amplitudes inside each exit-vector soli-

ton have switched. One interesting feature about Fig. 7(a) is that, as the collision-velocity V_0 approaches 0, the exit velocity does not approach zero. In other words, slow collision does not lead to slow separation. This is in contrast with Fig. 6(a) when $\beta=1.2$. Another phenomenon at $\beta=2$ is that, in a certain collision-velocity range (around the interval [0.2, 0.6]), a third vector soliton with zero velocity and low amplitude appears as well. Below or above this velocity range, we did not observe this third soliton.

As β increases above two, there is no qualitative change in the collision process. A quantitative difference is just that, at larger β values, the third vector soliton appears in wider collision-velocity intervals. At sufficiently large β values, even the fourth or more vector solitons may appear.

III. THE VARIATIONAL MODEL

How can we analytically explain the emergence of window sequences and fractal structures reported in the previous section? Given the wide spectrum of collision behaviors at various β values, this will not be a easy task. However, at small β values, this study is indeed possible. The observation we make is that, at small β values, there is little pulse splitting during collisions (see Figs. 1, 2, and 3). Each of the solitons (2.7) and (2.8) still remains as a single pulse, but its width and amplitude may oscillate considerably. This suggests to us a variational approach where we take an ansatz for each soliton that accounts for width and amplitude variations as well as position and velocity variations. Since initial solitons (2.7) and (2.8) have sech profiles and collisions are not violent at small β values, it makes sense to adopt the following sech ansatz for solitons throughout collision

$$A(x,t)=\sqrt{2}a_1\,\mathrm{sech}\left(\frac{x-\xi_1}{w_1}\right)e^{i[v_1/2(x-\xi_1)+b_1/2w_1(x-\xi_1)^2+\sigma_1]}, \tag{3.1}$$

$$B(x,t)=\sqrt{2}a_2\,\mathrm{sech}\left(\frac{x-\xi_2}{w_2}\right)e^{i[v_2/2(x-\xi_2)+b_2/2w_2(x-\xi_2)^2+\sigma_2]}, \tag{3.2}$$

where a_k, w_k, ξ_k, v_k, b_k, and $\sigma_k(k=1,2)$ are the solitons' amplitude, width, position, velocity, chirp, and phase, which are all functions of time t. The chirp term is introduced to induce width and amplitude oscillations. The Lagrangian of the governing Eqs. (2.1) and (2.2) is

$$L=\int_{-\infty}^{\infty}\mathcal{L}(A,B)dx, \tag{3.3}$$

where the Lagrangian density $\mathcal{L}$ is

$$\mathcal{L}=i(AA_t^*-A_tA^*)+i(BB_t^*-B_tB^*)+(2|A_x|^2-|A|^4)+(2|B_x|^2-|B|^4)-2\beta|A|^2|B|^2, \tag{3.4}$$

and superscript ''*'' represents complex conjugation. When the ansatzs (3.1) and (3.2) are substituted into the Lagrangian (3.3) and variations with respect to each of the soliton parameters taken, a system of ODE's for these soliton parameters will be derived. In our situation, the two solitons are always symmetric due to initial conditions (2.7) and (2.8). Thus, the following relations hold at all times

$$\xi_1=-\xi_2\equiv-\frac{\Delta}{2},\quad v_1=-v_2\equiv\frac{v}{2},\quad b_1=b_2\equiv b,$$

$$w_1=w_2\equiv w,\quad a_1=a_2\equiv a. \tag{3.5}$$

Here, Δ is the pulse center-position separation, and v is the relative velocity between the two pulses. Utilizing these relations, the ODE's for separation Δ, relative velocity v, width w, and chirp b simply become

$$\frac{d\Delta}{dt}=v, \tag{3.6}$$

$$\frac{dv}{dt}=\frac{16K\beta}{w^2}F'(\alpha), \tag{3.7}$$

$$\frac{dw}{dt}=2b, \tag{3.8}$$

$$\frac{db}{dt}=\frac{8}{\pi^2w^2}\left\{\frac{1}{w}-K-3\beta K[\alpha F(\alpha)]'\right\}, \tag{3.9}$$

where

$$F(\alpha)=\frac{\alpha\cosh\alpha-\sinh\alpha}{\sinh^3\alpha}, \tag{3.10}$$

and

$$\alpha=\frac{\Delta}{w},\quad K=a^2w=\text{const.} \tag{3.11}$$

Corresponding to the initial solitons (2.7) and (2.8), the initial conditions for the above ODE's are

$$\Delta(0)=\Delta_0,\quad v(0)=V_0,\quad w(0)=a(0)=1,\quad b(0)=0,\quad K=1. \tag{3.12}$$

We note that the above variational model and ODE's (3.6) to (3.9) have been derived before by Ueda and Kath [38] to study internal oscillations of vector solitons when initial pulses (2.7) and (2.8) overlap with each other. Here, we use this model to study the collision of these pulses where they are initially far apart but moving toward each other.

At a given β value, we integrate ODE's (3.6) to (3.9) numerically by the adaptive Runge-Kutta-Fehlberg method for various collision-velocities V_0. The initial separation Δ_0 may be chosen as any large value. To be consistent with our numerical simulations in the previous section, we select $\Delta_0=20$ throughout this section. The exit-velocity V is the $v(t)$ value after the collision has completed and the solitons (3.1) and (3.2) have separated far apart again $[\Delta(t)\gg1]$. Interpretation of an ODE solution requires caution however. According to these ODE's, solitons (3.1) and (3.2) almost always separate after a sufficiently long time. The reason is that our

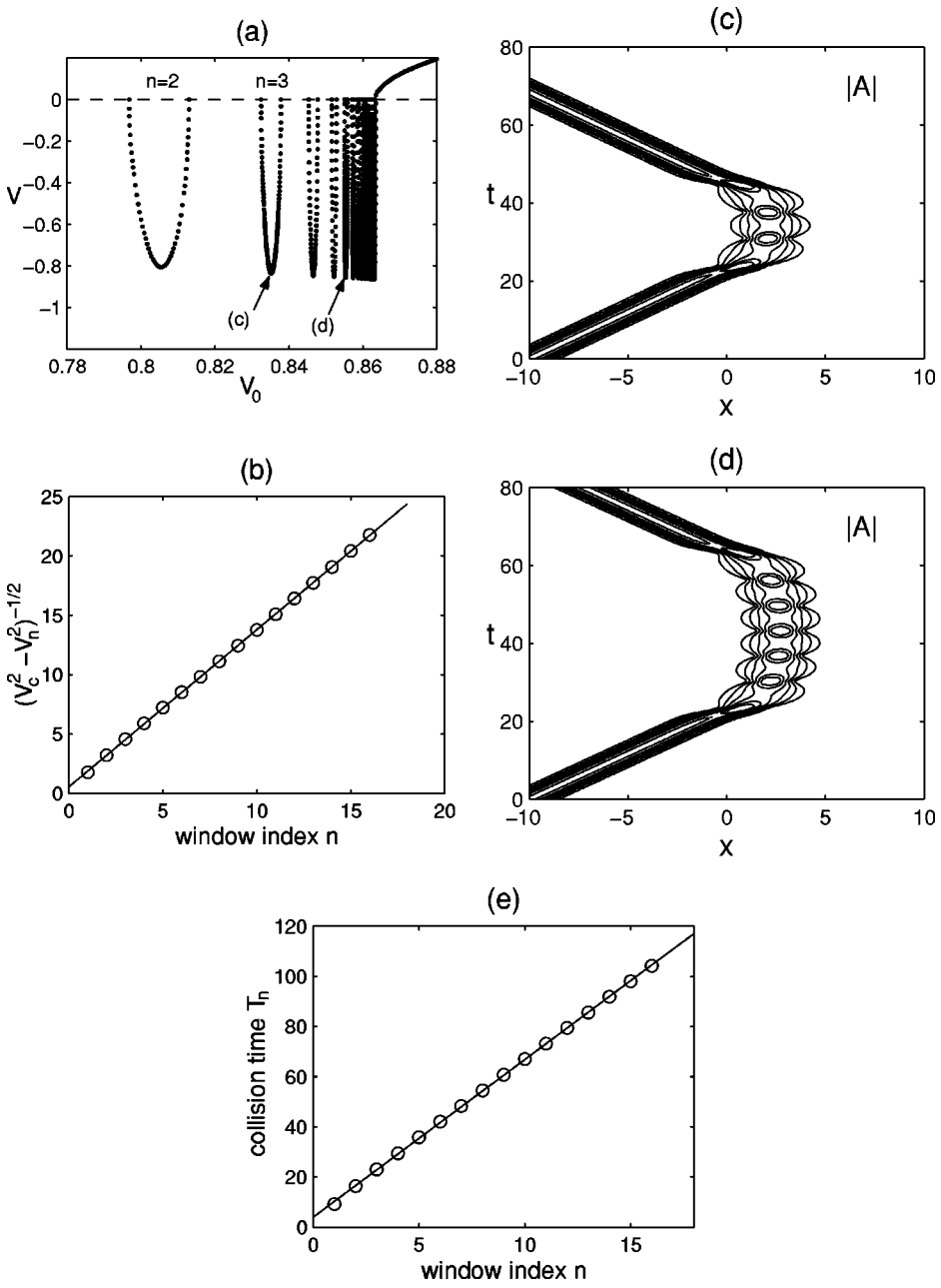

FIG. 8. Collision results for $\beta = 0.2$ in the variational model. (a) Exit-velocity graph. (b) $(V_c^2 - V_n^2)^{-1/2}$ graph (circles). The solid line is the least-squares fit given by Eqs. (2.9) and (3.13). (c,d) $|A|$ ansatz contours with V_0 at the bottoms of the second and fifth windows with indices $n=3$ and 6 in (a). Contour levels are both 0.6:0.15:1.35. (e) Collision time graph (circles). The solid line is the least-squares fit given by Eqs. (2.11) and (3.14).

variational model does not allow any energy radiation. Thus, these solitons always have enough energy to escape from each other, and they almost always do so when timing is right. But, if an ODE solution is such that solitons (3.1) and (3.2) cross each other many times before they eventually separate, in reality, that collision should be considered as trapping because energy loss to radiation during these crossings would be large enough that solitons become unable to escape from each other (see Fig. 3). In view of this, we will only look for ODE solutions with a small number of soliton crossings. Comparatively, width and amplitude oscillations (breathing) of a soliton does not generate much radiation [see Figs. 2(c) and 2(d)]. Thus, the ODE solution is still valid after a large number of such oscillations.

Our extensive numerical study of the ODE model (3.6) to (3.9) shows that at small β values, there is a critical-velocity V_c above which all collisions are transmissional. Below V_c, a sequence of two-pass reflection windows exists. In the following, we report these results for $\beta = 0.2$ and compare them to numerical results in Sec. II. Restricting the number of passes between solitons in the ODE model to be less or equal to two, the exit-velocity versus collision-velocity graph is then shown in Fig. 8(a). In this figure, we see a sequence of reflection windows just like Fig. 2(a) of the PDE system. Contour plots of $|A|$ ansatz (3.1) at the bottoms of the second and fifth windows (with indices $n=3$ and 6) in Fig. 8(a) are displayed in Figs. 8(c) and 8(d), respectively (it is noted that the $|B|$ contour is simply a mirror reflection of the $|A|$ contour). These contours show that in both windows, solitons (3.1) and (3.2) pass each other twice, but numbers of width oscillations between passes are different. Obviously, these collision dynamics are qualitatively identical to those in Figs.

2(c) and 2(d), which confirms that the window sequence in Fig. 8(a) is indeed the sequence of two-pass windows. One minor difference between collisions in the variational model and those in the PDE system is that, in the variational model, the simplest two-pass window with index $n=1$ appears at [0.7967, 0.8129] [outside the interval range of Fig. 8(a)]. Comparatively, that window has not been born yet in the PDE system [see Fig. 2(a)].

Other aspects of collision structure and dynamics in the variational model at $\beta=0.2$ closely resemble those in the PDE system as well. First, we look at window locations in Fig. 8(a). Here, the critical-velocity $V_c=0.863\,38$. In each reflection window, we take its midpoint V_n. Then we plot the quantity $(V_c^2-V_n^2)^{-1/2}$ versus window index n in Fig. 8(b). Clearly, $(V_c^2-V_n^2)^{-1/2}$ here is also a linear function of n, just like in the PDE case [see Fig. 2(b)]. A least-squares line fit shows that the slope μ_v and y-intercept θ_v of the linear function (2.9) now is

$$\mu_v=1.3234, \quad \theta_v=0.5496, \tag{3.13}$$

which are a little different from the true values given in Eq. (2.10). Second, we examine collision times at bottoms of these reflection windows. The collision time here is naturally defined as the time between the two position intersections of the A and B ansatzs (3.1) and (3.2). Not surprisingly, we find that collision time T_n is also a linear function of the window index n in the same form of Eq. (2.11), and a least-square line fit shows that the frequency ω_v and offset parameter δ_v now are

$$\omega_v=0.9993, \quad \delta_v=3.9494, \tag{3.14}$$

which are again a little different from those in Eq. (2.12) for the PDE system.

Differences between the variational model and true collision dynamics are mostly quantitative. Comparing Figs. 2(a) to Fig. 8(a), locations of reflection windows are a little off from each other. Coefficients in linear functions (2.9) and (2.11) are different too. But the variational model has clearly captured the key collision structure and dynamics of the original PDE system qualitatively.

In collisions of the PDE system at $\beta=0.2$, transmission windows at edges of two-pass reflection windows never appeared, even though their ''quasiexistence'' was suggested by collision contours in Fig. 3. In the variational model, we find that such edge windows do appear. To illustrate, let us choose the second two-pass window in Fig. 8(a) (with index $n=3$), as we did in Fig. 3. Below its left edge, we discovered a sequence of three-pass transmission windows. These edge windows are shown in Fig. 9(a). Picking the second and sixth transmission windows as marked by letters ''(b)'' and ''(c),'' we show their peak-point ansatz contours (3.1) in Figs. 9(b) and 9(c), respectively. In both collisions, solitons pass each other three times, but numbers of width oscillations between the second and third passes are different. This characteristic is true of all the edge windows in Fig. 9(a). Thus, these windows do belong to the same sequence of three-pass windows. Comparing contours in Fig. 9 to those

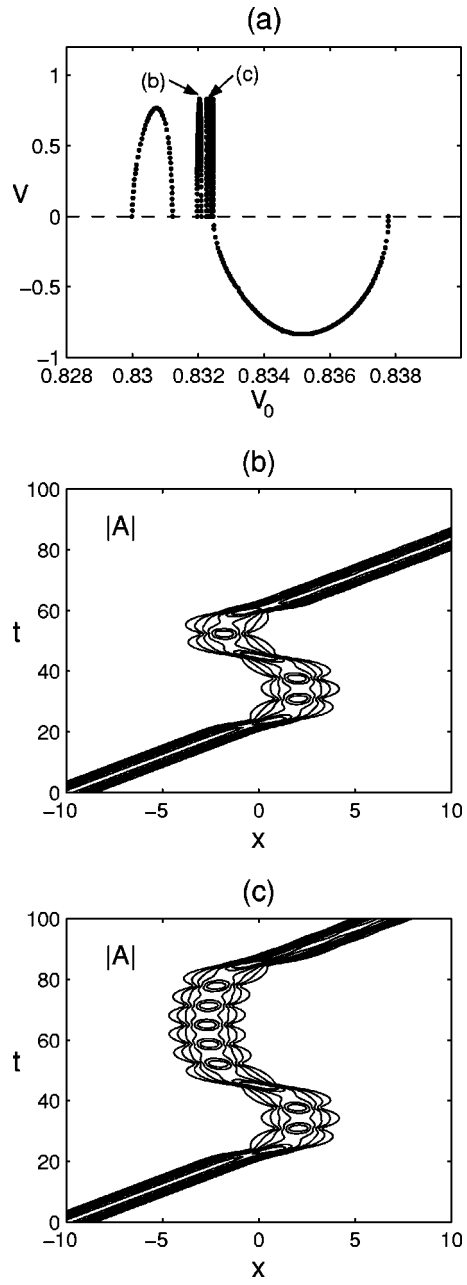

FIG. 9. Edge windows and their dynamics just below the $n=3$ reflection window of Fig. 8(a) in the variational model. (a) Edge windows; (b,c) $|A|$-ansatz contours with V_0 at peaks of the second and sixth transmission windows marked by respective letters in (a); contour levels are both 0.6:0.15:1.35.

in Fig. 3, we see that they are quite similar, except that solitons in Fig. 3 trap each other instead of escaping from each other after the third pass. Since the main difference between the variational model and the PDE system is that the variational model does not allow energy radiation, while the PDE system does, we conclude that the eventual trapping of solitons in Fig. 3 is caused by energy radiation. In other words, energy radiation wipes out edge windows of the PDE system.

As β increases, other windows of more complex collisions gradually emerge in the ODE model. This process

closely mirrors that in the PDE system. The ability of the variational model to qualitatively reproduce true collision dynamics of the PDE system indicates that our variational ansatzs have fully or partially captured the main features of true collisions. In the variational model, width oscillations play a critical role, and the resonance between width oscillations and translational motion of solitons is responsible for the rich collision structures. For soliton collisions in the PDE system, at small β values, this resonance appears to be the only mechanism for the creation of the two-pass window sequence (see Fig. 2). At moderate β values, pulse splitting during collisions produces two nondegenerate vector solitons. Then oscillations of relative positions between two components inside each vector soliton may also get involved in the resonance mechanism [27,28]. Incorporation of position oscillations into the variational model may be done, but it is fairly complicated. Thus, it will not be pursued in this article.

IV. COLLISION DEPENDENCE ON POLARIZATION

The collisions studied in previous two sections are between vector solitons of orthogonal polarizations and equal amplitudes [see Eqs. (2.7) and (2.8)]. Such collisions are rather special. In practical situations, it is quite likely that initial solitons are not orthogonally polarized, or they have different amplitudes. Thus, an important question is how the collision structure of previous sections changes when initial solitons become nonorthogonally polarized or have different amplitudes. This question will be addressed in this and the next sections.

In this section, we study how the collision structure and dynamics change when initial vector solitons are not orthogonal, i.e., their initial polarization angles are not 0 and $\pi/2$. For this purpose, we take the initial condition as

$$A(x,0)=r_1\left(x+\frac{\Delta_0}{2}\right)e^{(1/4)iV_0x}+r_2\left(x-\frac{\Delta_0}{2}\right)e^{-(1/4)iV_0x+i\gamma_1}, \tag{4.1}$$

$$B(x,0)=r_2\left(x+\frac{\Delta_0}{2}\right)e^{(1/4)iV_0x}+r_1\left(x-\frac{\Delta_0}{2}\right)e^{-(1/4)iV_0x+i\gamma_2}, \tag{4.2}$$

where $\Delta_0(\gg 1)$ is the initial vector-soliton separation, V_0 is the collision velocity, and (γ_1,γ_2) are initial relative phases of the two solitons in the A and B components. Functions $[r_1(x),r_2(x)]$ are nondegenerate vector solitons with frequencies (ω_1^2,ω_2^2), and they satisfy the ODE systems (2.5) and (2.6). By rescaling variables, we can always normalize $\omega_1=1$. As we have mentioned in Sec. II, in order to get a nondegenerate single-hump vector soliton, the frequency ratio ω_2/ω_1 must lie inside the interval $[(\sqrt{1+8\beta}-1)/2,2/(\sqrt{1+8\beta}-1)]$. At the end points of this interval, the vector soliton is degenerate again, and initial conditions (4.1) and (4.2) reduce to Eqs. (2.7) and (2.8). It is noted that the two polarized vector solitons in Eqs. (4.1) and (4.2) have the same total energy. In addition, they satisfy the symmetry $A(x,0)=B(-x,0)$ if $\gamma_1=\gamma_2=0$. This initial symmetry guarantees that the solution holds this same symmetry at all times. This feature is the same as initial conditions (2.7) and (2.8).

For collisions of nondegenerate vector solitons, initial relative phases between the two solitons may no longer be removed, and they will affect the collision in a nontrivial way. This is why we introduced such phases (γ_1 and γ_2) in initial conditions (4.1) and (4.2) in the first place. Another feature is that collisions of nondegenerate vector solitons depend on initial position separation Δ_0 as well, no matter how large is Δ_0. The reason is simple to explain. Suppose the initial separation has been changed from Δ_0 to Δ_0+h. At collision-velocity V_0, it takes extra time h/V_0 for vector solitons to move to the original separation Δ_0. During this time, the A component of the left vector soliton has gained a phase increase $(\omega_1^2-V_0^2/16)h/V_0$ [see Eq. (2.3)], while the same component of the right vector soliton has gained a phase increase $(\omega_2^2-V_0^2/16)h/V_0$. Thus, the A-component phase difference at separation Δ_0 is $\gamma_1+(\omega_2^2-\omega_1^2)h/V_0$ instead of γ_1. Similarly, the B-component phase difference at separation Δ_0 is $\gamma_2-(\omega_2^2-\omega_1^2)h/V_0$ instead of γ_2. Due to phase dependence of collisions, it is evident that the collision at separation Δ_0+h is generally different from that at separation Δ_0. The above argument also shows that, under the transformation

$$\Delta_0\to\Delta_0+h,\quad \gamma_1\to\gamma_1-(\omega_2^2-\omega_1^2)\frac{h}{V_0},$$

$$\gamma_2\to\gamma_2+(\omega_2^2-\omega_1^2)\frac{h}{V_0}, \tag{4.3}$$

the collision remains the same as long as $\Delta_0\gg 1$.

We have carried out collision simulations at $\beta=2/3$ with initial phases $\gamma_1=\gamma_2=0$ and vector-soliton frequencies $\omega_1=1$ and $\omega_2=0.78$. The initial separation Δ_0 is allowed to vary so that collision dependence on Δ_0 may be assessed. First, we take $\Delta_0=40$. For these system parameters, the initial vector solitons (4.1) and (4.2) are displayed in Fig. 10(a). As we can see, each vector soliton here has a wave-shadow structure [15], and the two vector solitons are weakly nonorthogonal. It turns out that even a weak nonorthogonality has a profound effect on collision structure and dynamics. In Fig. 10(b), the exit-velocity versus collision-velocity graph is displayed. Clearly, this graph is quite different from that where initial solitons were perfectly orthogonal [27,28]. Its structure is simpler than the orthogonal case. The jump at $V_0=1.30$ here is similar to those in Figs. 6(a) and 7: below the jump, slightly more energy is reflected; above the jump, slightly more energy is transmitted.

A feature of Fig. 10(b) is the appearance of a sequence of reflection windows on the left-hand side of the graph. This window sequence is fundamentally different from that in Fig. 2(a) on the geometrical feature, dynamics, and mechanism. Geometrically, this window sequence converges toward the left. The first window in this sequence with index $n=1$ is

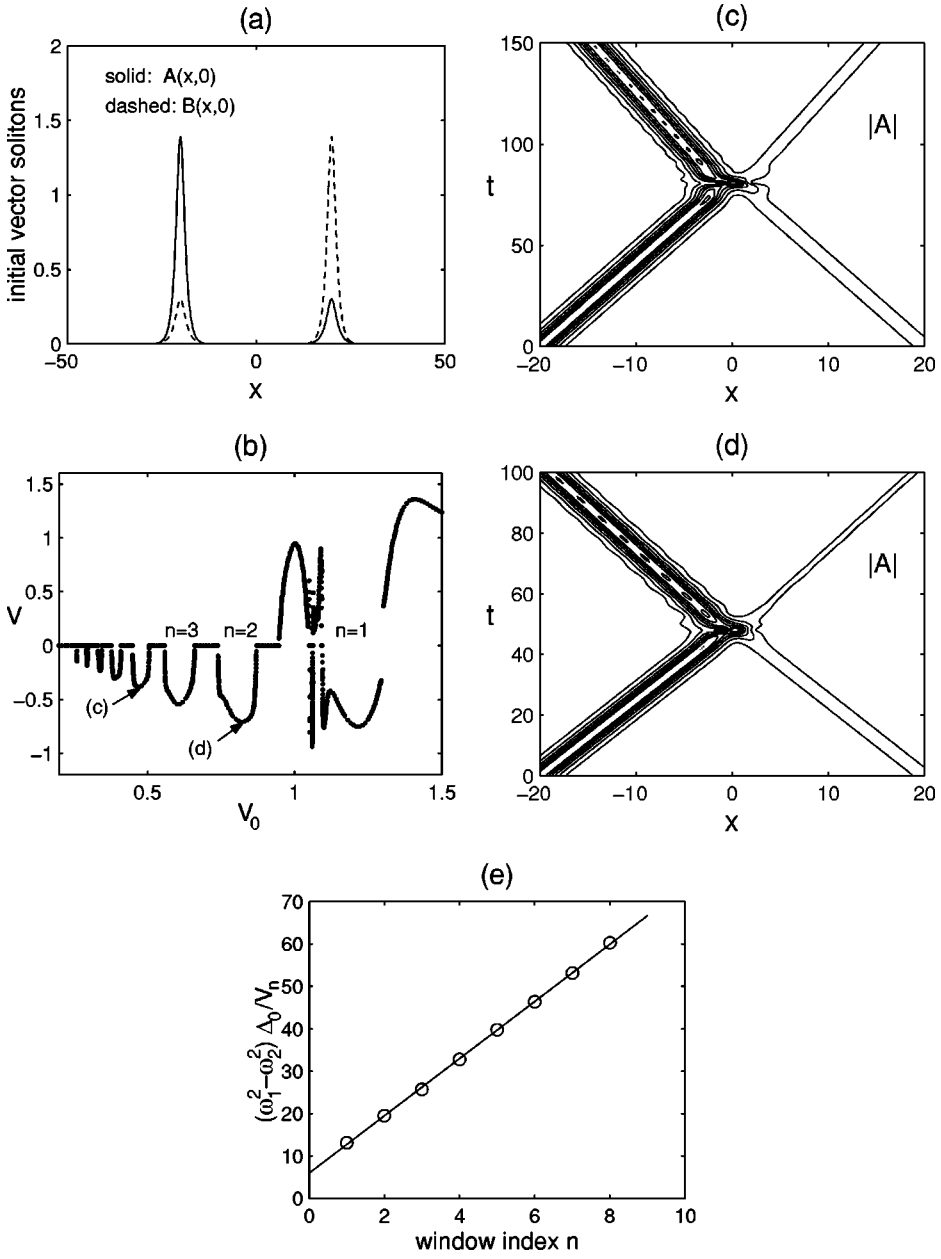

FIG. 10. Collision results of weakly nonorthogonal vector solitons at $\beta=2/3$. The initial condition is Eqs. (4.1) and (4.2) with $\omega_1=1$, $\omega_2=0.78$, $\Delta_0=40$, and $\gamma_1=\gamma_2=0$. (a) The initial condition $A(x,0)$ (solid) and $B(x,0)$ (dashed); (b) the exit velocity graph; (c,d) $|A|$ contours with V_0 at midpoints of the $n=4$ and 2 windows in (b); both contours are 0.2:0.2:1.4; (e) $(\omega_2^2-\omega_1^2)\Delta_0/V_n$ graph (circles). The solid line is the least-squares fit given by Eqs. (4.4) and (4.5).

located at [1.0948, 1.2944]. The next window with index $n=2$ is at [0.7400, 0.8698]. Higher-indexed windows are further to the left. Dynamically, collisions in all windows in this sequence are simple one-bounce collisions. To demonstrate, we show in Figs. 10(c) and 10(d) collision contours at the midpoints of the $n=4$ and $n=2$ windows as marked by respective letters. Only $|A|$ contours are shown because the reflectional symmetry $B(x,t)=A(-x,t)$ still holds here. As we can see from these contours, both collisions are simple reflections. Their similarity is obvious. Collision contours in other windows of this sequence are similar.

What mechanism creates this sequence of reflection windows? Apparently, the mechanism here is not the resonance discussed in previous sections. The similarity of collisions in these windows offers the following answer. When a vector soliton travels, its phases change according to Eqs. (2.3) and (2.4), thus, these phases at the soliton center $x=vt+x_0$ are $(\omega_1^2+(1/4)v^2)t+(1/2)vx_0+\gamma_1$ for A and $(\omega_2^2+(1/4)v^2)t+(1/2)vx_0+\gamma_2$ for B. Now, when the two vector solitons in the initial conditions (4.1) and (4.2) move toward each other, the relative phases between their soliton centers are $(\omega_2^2-\omega_1^2)t$ for A and $-(\omega_2^2-\omega_1^2)t$ for B (note that $\gamma_1=\gamma_2=0$ in our choices of parameters). We know that collisions of nondegenerate vector solitons depend on relative phases. For vector solitons in Eqs. (4.1) and (4.2) with initial separation Δ_0 and collision-velocity V_0, collision occurs at $t\approx\Delta_0/V_0$. At this time of collision, the relative phases of soliton centers are $(\omega_2^2-\omega_1^2)\Delta_0/V_0$ for A and $-(\omega_2^2-\omega_1^2)\Delta_0/V_0$ for B. Our key observation is that, at two collision velocities, if the above relative phases at collision differ by a multiple of 2π, then the collision outcomes should be roughly the same (the reader is reminded that a vector soliton's amplitude profile remains the same at all velocities). Mathematically, it means that at collision velocities V_n $(n=1,2,\ldots,)$ where

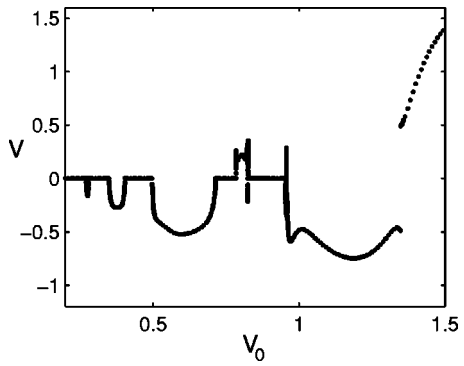

FIG. 11. Exit-velocity graph at initial separation $\Delta_0=20$. The other parameters in the initial conditions (4.1) and (4.2) are the same as in Fig. 10.

$$\frac{(\omega_2^2-\omega_1^2)\Delta_0}{V_n}=\tau n+\phi, \tag{4.4}$$

slope $\tau=2\pi$ and ϕ is a constant, collision dynamics should be about the same. To check this formula, we have determined the midpoints V_n of those reflection windows. When quantities $(\omega_2^2-\omega_1^2)\Delta_0/V_n$ are plotted in Fig. 10(e) versus window index n (circles), we see that the dependence is indeed linear. A least-square line fit shows that the actual slope τ and y-intercept ϕ in Eq. (4.4) are

$$\tau=6.7525, \quad \phi=5.9289. \tag{4.5}$$

The slope is rather close to the theoretical value 2π. This surprisingly good agreement confirms that this sequence of reflection windows is indeed caused by the phase dependence of collisions as described above. Furthermore, linear relation (4.4) does hold very well. We attribute the minor difference between the theoretical slope 2π and the actual slope 6.7525 to the fact that phase variations across each vector soliton, which depend on x in the form of $\pm(1/4)V_0x$, also affect the collision outcome. This effect is understandably small. The reason is that in this window sequence, V_0 is about one or smaller. In addition, the half width of each vector soliton, defined as one half of the full width at half maximum (FWHM), is about 0.88. Thus, phase variations across a vector soliton are about 0.22 or smaller. Consequently, differences of these phase variations at different collision velocities would be even smaller, thus, are insignificant compared to overall phase differences between the two solitons (which are multiples of 2π).

As we have said before, collisions of nonorthogonal vector solitons depend on initial separation Δ_0. To study this separation dependence, we now choose another separation value $\Delta_0=20$ while keeping the other system parameters the same. The exit-velocity graph for this case is shown in Fig. 11. This graph is somewhat similar to Fig. 10(b). However, it is a little simpler. There are less reflection windows in this sequence. Window locations are changed significantly too. The midpoints V_n of windows in this sequence satisfy the same relation (4.4), but the slope τ here is 7.2849, which is slightly different from that at $\Delta_0=40$.

The scope of collision dependence on polarizations reported in this section is rather limited. We only investigated this dependence at small polarization angles for one XPM coefficient $\beta=2/3$. However, the phase-induced sequence of reflection windows we have discovered is expected at other β values and different polarization angles as well, as phase dependence is present in such collisions too. Last, possibilities still exist that other interesting collision structures may arise in different parameter regions of polarization angles, relative initial phases and XPM coefficients. This remains to be seen.

V. COLLISION DEPENDENCE ON RELATIVE AMPLITUDES

Collision dependence on relative amplitudes of two-vector solitons is another important issue. This will be studied briefly in this section. To isolate this effect, we will again make initial vector solitons orthogonally polarized. Thus, we take the initial condition as

$$A(x,0)=\sqrt{2}a\ \mathrm{sech}\,a\left(x+\frac{1}{2}\Delta_0\right)e^{(1/4)iV_0x}, \tag{5.1}$$

$$B(x,0)=\sqrt{2}\ \mathrm{sech}(x-(1/2)\Delta_0)e^{-(1/4)iV_0x}, \tag{5.2}$$

where the right soliton's amplitude has been normalized to be $\sqrt{2}$, and a is the relative amplitude of the left soliton (in the orthogonal polarization). Note that for this collision, the symmetry $A(x,t)=B(-x,t)$ is lost, and the exit pulses generally have different velocities (in magnitude). Also, note that this collision now is independent of the initial position separation Δ_0 again as long as $\Delta_0\gg1$. We have simulated this collision at various collision-velocities V_0, relative amplitudes a, and XPM coefficients β. In these simulations, the initial separation is always taken as $\Delta_0=20$. The general conclusion is that when the amplitude difference between these solitons increases, the collision structure simplifies. To demonstrate, we select $\beta=2/3$ and $a=1.2$. For each collision, we found that two-vector solitons with velocities not opposite of each other emerge after collision. The velocities of these emerged solitons are displayed in Figs. 12(a) and 12(b). Obviously, these velocity graphs are very simplified compared to those in [27,28] where $a=1$. In fact, the fractal structure has disappeared now. At higher a values, the velocity graph would be even simpler. It is noted that the collision of solitons (5.1) and (5.2) has been studied before by the multisoliton perturbation method for the Manakov system [18]. The collision structure in Fig. 12 is consistent with the results of [18].

VI. DISCUSSION

In previous sections, we have presented a numerical and analytical study of vector-soliton collisions in the coupled nonlinear Schrödinger Eqs. (2.1) and (2.2). We have shown that for collisions of orthogonally polarized and equal-amplitude vector solitons, when the XPM coefficient β is small, a sequence of reflection windows similar to that in the

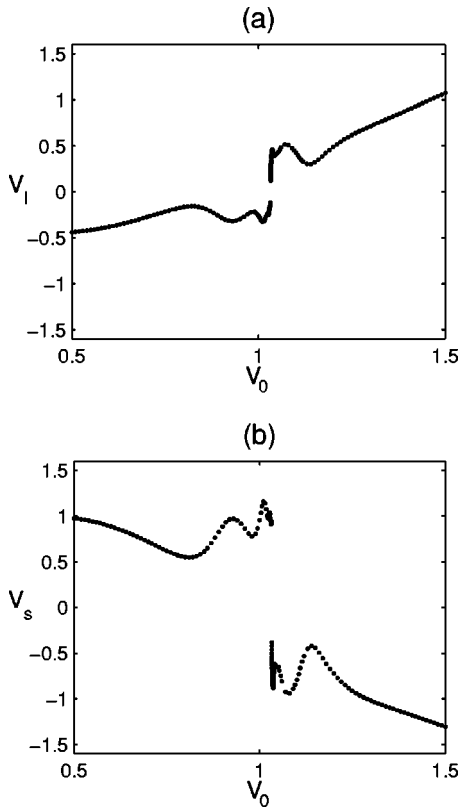

FIG. 12. Collision results for solitons of unequal amplitudes at $\beta=2/3$. The initial condition is (5.1) and (5.2) with $a=1.2$. (a) Velocity V_l of the larger vector soliton emerged; (b) velocity V_s of the smaller vector soliton emerged.

ϕ^4 model arises. When β increases, a coupled NLS fractal gradually emerges. But when β is greater than one, this fractal disappears. Analytically, we have explained these collision behaviors by a variational model that qualitatively reproduces the main features of these collisions. This variational model indicates that these window sequences and fractal structures are caused entirely or partially by a resonance mechanism between the translational motion and width oscillations of vector solitons. We have also investigated collision dependence on initial polarizations, and discovered a sequence of reflection windows that is *phase induced*. Our analytical formula for the locations of these phase-induced windows agrees well with the numerical values. Last, we have examined collision dependence on relative amplitudes and showed that when vector solitons have different amplitudes, the collision structure simplifies.

There are three key collision structures in the coupled NLS Eqs. (2.1) and (2.2). The first one is the resonance-induced sequence of reflection windows similar to ϕ^4's in collisions of orthogonally polarized and equal-amplitude vector solitons at small β values [see Fig. 2(a)]. The second one is the coupled NLS fractal at moderate β values [see Fig. 4(a) and [27,28]]. The third is a phase-induced sequence of reflection windows in collisions of nonorthogonally polarized vector solitons (see Fig. 10). The first structure has been discovered in many sine-Gordon-type equations [21–25]. Its reappearance in the coupled NLS system suggests its universality. The second structure is a fractal that is distinctively different from ϕ^4's. Its basic structure is a collection of multipass and multibounce windows. Whether this coupled NLS fractal can reappear in other wave systems remains an interesting question. On the other hand, these two structures are intimately related at least in the coupled NLS system in two respects: (1) the first structure bifurcates into the second one as β continuously increases; (2) the mechanisms for both structures are resonances between translational motion and internal oscillations of vector solitons. The third structure is unrelated to the first two: it is phase induced, and its collision dynamics is different.

It is noted that only the main collision structures are reported in this article. Some minor features have been omitted. For instance, in collisions of orthogonally polarized and equal-amplitude vector solitons, as β steadily increases, some reflection or transmission windows may mysteriously appear out of nowhere, then disappear with no trace left. Results on polarization rotation (shadow formation) and amplitude changes after collision are omitted too.

Last, we discuss potential experimental verifications of our results. The model Eqs. (2.1) and (2.2) we have studied are widely accepted as governing pulse propagations in birefringent nonlinear optical fibers [29] (without random birefringence). For fibers of linear birefringence, the XPM coefficient is $\beta=2/3$ [29]. For elliptical birefringence, β can take other values [30]. The dimensionless collision velocity V_0 in our model is related to physical parameters as [29]

$$V_0=\frac{4\pi\Delta n}{\lambda^2|D|}\times\frac{\tau}{1.763}, \tag{6.1}$$

where Δn is the index difference of the fiber's two polarizations, τ is the pulse's FWHM, λ is the wavelength, and D is the dispersion parameter (note that D in [29] was defined differently). For step-index single-mode fibers, the typical value for D is 15.6 ps/nm/km at wavelength $\lambda=1.55$ μm [1]. According to [44], Δn varies between 5×10^{-9} and 8×10^{-4}. Typical values concentrate in the range 10^{-6} to 10^{-5}. If we let $\tau=5$ ps, then the total range for V_0 is from 4.8×10^{-3} to 7.6×10^{2}, while typical values fall between 0.95 and 9.5. Many of the interesting collision structures discovered in this paper such as the resonance-induced sequence of reflection windows in Fig. 2(a), the coupled NLS fractal in Fig. 4 and [27,28], and the phase-induced sequence of reflection windows in Fig. 10(b) fall entirely or partially in the range of typical experimental parameters. Equally importantly, some of these windows such as those induced by phase in Fig. 10(b) are very wide, so they should survive under inevitable birefringence fluctuations in real experiments. Thus, experimental observation of collision results in this paper is quite feasible.

ACKNOWLEDGMENTS

The authors thank T.I. Lakoba for a careful reading of the manuscript. This work was supported in part by the U.S. Air Force Office of Scientific Research under Contract No. F49620-99-1-0174, and by the National Science Foundation under Grant No. DMS-9971712.

[1] G. P. Agrawal, *Nonlinear Fiber Optics* (Academic Press, San Diego, 1989).
[2] A. Hasegawa and Y. Kodama, *Solitons in Optical Communications* (Clarendon, Oxford, 1995).
[3] L. F. Mollenauer, J. P. Gordon, and F. Heismann, Opt. Lett. **20**, 2060 (1995).
[4] A. W. Snyder and A. P. Sheppard, Opt. Lett. **18**, 482 (1993).
[5] M. Shih, Z. Chen, M. Segev, T. H. Coskun, and D. N. Christodoulides, Appl. Phys. Lett. **69**, 4151 (1996).
[6] H. Meng, G. Salamo, M. Shih, and M. Segev, Opt. Lett. **22**, 448 (1997).
[7] Y. Baek, R. Schiek, G. I. Stegeman, I. Baumann, and W. Sohler, Opt. Lett. **22**, 1550 (1997).
[8] W. Krolikowski and S. A. Holmstrom, Opt. Lett. **22**, 369 (1997).
[9] W. Krolikowski, B. Luther-Davies, C. Denz, and T. Tschudi, Opt. Lett. **23**, 97 (1998).
[10] C. Anastassiou, M. Segev, K. Steiglitz, J. A. Giordmaine, M. Mitchell, M. Shih, S. Lan, and J. Martin, Phys. Rev. Lett. **83**, 2332 (1999).
[11] M. J. Ablowitz and H. Segur, *Solitons and the Inverse Scattering Transform* (SIAM, Philadelphia, 1981).
[12] B. A. Malomed and S. Wabnitz, Opt. Lett. **16**, 1388 (1991).
[13] B. A. Malomed, J. Opt. Soc. Am. B **9**, 2075 (1992).
[14] C. Etrich, U. Peschel, and B. A. Malomed, Phys. Rev. A **52**, R3444 (1995).
[15] J. Yang and D. J. Benney, Stud. Appl. Math. **96**, 111 (1996).
[16] V. V. Steblina, Y. S. Kivshar, and A. V. Buryak, Opt. Lett. **23**, 156 (1998).
[17] A. V. Buryak, Y. S. Kivshar, M. Shih, and M. Segev, Phys. Rev. Lett. **82**, 81 (1999).
[18] J. Yang, Phys. Rev. E. **59**, 2393 (1999).
[19] B. Tan and J. P. Boyd, Chaos, Solitons and Fractals (to be published).
[20] S. V. Dmitriev, Y. S. Kivshar, and T. Shigenari (unpublished).
[21] D. K. Campbell, J. F. Schonfeld, and C. A. Wingate, Physica D **9**, 1 (1983).
[22] M. Peyrard and D. K. Campbell, Physica D **9**, 33 (1983).
[23] D. K. Campbell, M. Peyrard, and P. Sodano, Physica D **19**, 165 (1986).
[24] Y. S. Kivshar, Z. Fei, and L. Lázquez, Phys. Rev. Lett. **67**, 1177 (1991).
[25] Z. Fei, Y. S. Kivshar, and L. Lázquez, Phys. Rev. A **46**, 5214 (1992).
[26] P. Anninos, S. Oliveira, and R. A. Matzner, Phys. Rev. D **44**, 1147 (1991).
[27] J. Yang and Y. Tan, Phys. Lett. A **280**, 129 (2001).
[28] J. Yang and Y. Tan, Phys. Rev. Lett. **85**, 3624 (2000).
[29] C. R. Menyuk, IEEE J. Quantum Electron. **QE-23**, 174 (1987).
[30] C. R. Menyuk, IEEE J. Quantum Electron. **QE-25**, 2674 (1989).
[31] M. Haelterman, A. P. Sheppard, and A. W. Snyder, Opt. Lett. **18**, 1406 (1993).
[32] M. Haelterman, A. P. Sheppard, and A. W. Snyder, Opt. Commun. **103**, 145 (1993).
[33] J. Yang, Physica D **108**, 92 (1997).
[34] J. Yang, Phys. Rev. E **64**, 026607 (2001).
[35] V. E. Zakharov and A. B. Shabat, Zh. Éksp. Teor. Fiz. **61**, 118 (1971) [Sov. Phys. JETP **34**, 62 (1972)].
[36] S. V. Manakov, Zh. Éksp. Teor. Fiz. **65**, 1392 (1973) [Sov. Phys. JETP **38**, 248 (1974)].
[37] R. Radhakrishnan, M. Lakshmanan, and J. Hietarinta, Phys. Rev. E **56**, 2213 (1997).
[38] T. Ueda and W. L. Kath, Phys. Rev. A **42**, 563 (1990).
[39] D. J. Kaup, B. A. Malomed, and R. S. Tasgal, Phys. Rev. E **48**, 3049 (1993).
[40] J. Yang, Stud. Appl. Math. **98**, 61 (1997).
[41] B. A. Malomed and R. S. Tasgal, Phys. Rev. E **58**, 2564 (1998).
[42] D. E. Pelinovsky and J. Yang, Stud. Appl. Math. **105**, 245 (2000).
[43] E. A. Kuznetsov, A. V. Mikhailov, and I. A. Shimokhin, Physica D **87**, 201 (1995).
[44] I. P. Kaminow, IEEE J. Quantum Electron. **QE-17**, 15 (1981).